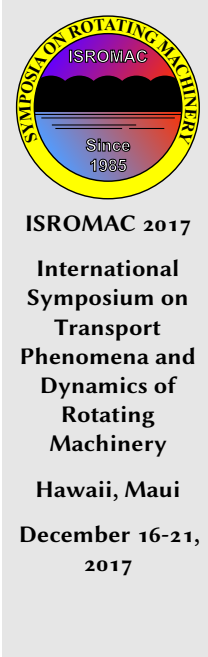


# Thermodynamic and Rotordynamic Assessment of Conventional and Ultra-High Bypass Ratio Engines

Thomas Müller<sup>1\*</sup>, Daniel Giesecke<sup>2</sup>, Jens Friedrichs<sup>2</sup>, Holger Hennings<sup>1</sup>



## Abstract

Due to the economical aspiration to increase the efficiency and several ecological regulations to reduce  $CO_2$  and noise emissions, aircraft and engine manufacturer have to increase the bypass ratio of gas turbines. But, the higher the bypass ratio of a gas turbine is the larger the rotating masses are. Thus, concerning the system stability due to the change of the eigenbehavior of the aircraft in its structure, the dynamic influences of gyroscopic moments as the consequence of the angular momentum of the engine are an uncertainty and need to be investigated carefully. This paper compares two gas turbines, a conventional one with a bypass ratio of 5 and one with an ultra-high bypass ratio of 17. Two different approaches are presented. On the one hand, a comparison regarding the thermodynamical cycle process, on the other hand, using a multibody formulation, a model of a Coanda wing with each of the engines mounted over the airfoil is presented. The analysis conducts the structural coupling and dynamical influences on the wing structure arising during their operation at specific design points. The comparison of the dynamic influences should show which structural effects on the wing structure come along with the trade-off due to increased thermodynamic efficiency.

## Keywords

Multibody Dynamics – Thermodynamic Efficiency – Gyroscopy – UHBR

<sup>1</sup> Institute of Aeroelasticity, German Aerospace Center, Germany

<sup>2</sup> Institute of Jet Propulsion and Turbomachinery, TU Braunschweig, Germany

\*Corresponding author: T-SMueller@dlr.de

## NOMENCLATURE

### Symbols

$[]$	matrix
$\{\}$	vector
$D$	damping matrix
$F$	force
$J$	moments of inertia
$L$	angular momentum
$m_u d$	unbalance mass at distance $d$
$M$	mass matrix
$M_i$	moment in $i$ -direction
$p$	external force
$P$	pressure
$S$	stiffness matrix
$T$	transformation matrix
$V$	velocity
$u, v$	vector for spatial coordinates
$x, y, z$	spatial coordinates
$\eta$	efficiency
$\psi, \theta$	tilting angle
$\Phi$	modal matrix
$\omega$	eigenfrequency
$\Omega$	rotational velocity

### Subscripts

18, *ideal* ideal bypass nozzle

8, *ideal* ideal core nozzle

$amb$	ambient
$a$	axial
$an$	antimetric
$p$	polar
$red$	reduced
$sy$	symmetric
$T$	transposed

### Abbreviations

ACARE	Advisory Council for Aeronautics Research in Europe
AEO	all engine operating
BPR	bypass ratio
CRC	Coordinated Research Centre
FPR	fan pressure ratio
GR	gear ratio
HPC	high pressure compressor
HPT	high pressure turbine
LPT	low pressure turbine
OEI	one engine inoperative
OPR	overall pressure ratio
PR	pressure ratio
ROM	reduced order model
SFC	specific fuel consumption
TET	turbine entry temperature
TOC	top of climb
UHBR	ultra-high bypass ratio

## INTRODUCTION

In the framework of the Coordinated Research Centre 880 (CRC 880) "Fundamentals of High Lift for Future Civil Aircraft" a future oriented aircraft is developed. It has a maximum payload of 12000 *kg* for 100 passengers and freight. The flight mission has to reach 2000 *km* flight range with additional fuel for alternative and holding flights. Furthermore, a runway length of more than 900 *m* is not allowed to exceed in order to use regional airports.

Moreover, economical demands such as the reduction of fuel consumption, and social-ecological demands, e.g.  $CO_2$  and noise emission, have to be taken into account to achieve a competitive design for short-haul missions. The idea is to relieve main hub airports by using regional airports, which are situated all over Europe. Additionally, this would allow faster point-to-point connections. However, increasing the air traffic around regional airports requires lower noise emissions as mentioned above. Hence, the aim of this project is in accordance to the guidelines defined by the Advisory Council for Aeronautics Research in Europe (ACARE) named "A Vision for 2020" [1] and "Flightpath 2050" [2]. In order to achieve the defined goals the CRC 880 is divided in four main research areas with corresponding projects in the research areas "Aeroacoustics Basics", "Efficient High-Lift", "Flight Dynamics" and "Aircraft Design and Technology Assessment".

In the field of "Efficient High-Lift", a geared ultra-high bypass ratio engine was developed. Increasing the bypass ratio has the beneficial effect on the propulsive efficiency of the engine leading to lower fuel consumption. This is a result of the enhanced propulsion efficiency when having a low specific thrust cycle. Dagget et al. [3] performed a diameter study by gradually increasing bypass ratio (BPR) from 14.3 to 21.5. Thereby, two different engine variants were investigated: a geared and an advanced counter-rotating turbofan mounted on a Boeing 777-200 aircraft. An aircraft assessment with three different General Electric and three different Pratt & Whitney engines including weight, drag, noise, emission, fuel consumptions and operating costs were performed. For each of the two engine architectures, one optimal BPR was estimated. Engine BPR of up to 14.5 were identified for one engine variant to achieve optimal parameters. Depending on the engine type, higher BPR leads to fuel costs reductions of up to 16%. However, Dagget et al. [3] indicated that larger diameter result in higher structural difficulty and loads aircraft wings have to cope with.

Hall and Crichton [4] designed four different ultra-high bypass (UHBR) turbofan engines for a blended wing body aircraft. The engine variants differ significantly in its mechanical design. However, all four engine configurations share the cycle parameters with the top of climb (TOC) as the design point.

An increased engine bypass ratio of 15.5 with an overall pressure ratio (OPR) of 57.4 and a fan pressure ratio (FPR) of 1.45 was chosen for the cycle design. This resulted in a specific fuel consumption (SFC) of 14.7 *g/sN*. A three spool conventional turbofan, a two spool geared turbofan, a two-spool engine with a slower fan and a multiple fan system with S-shape intake ducts over the aircraft were developed.

Subsequently, four different designs were assessed in a preliminary engine mechanical design study by considering noise, fuel burn, engine weight and aircraft integrity.

The multiple fan system, one possible future variant investigated in Hall and Crichton [4], is expected to get easier installed into the airframe structure. Reference [4] concluded that both, the multiple fan variant and the two spool geared turbofan configurations are expected to emit lower noise and reduce engine weight.

As a conclusion of the engine design study from Hall and Crichton [4] and the statement in Dagget et al. [3] regarding larger diameter and its structural difficulty on aircraft wings, the larger rotating masses have to be taken into account in further detail. Increasing the rotating masses proportionally scales the angular momentum of the engine. A change in the direction of the angular momentum due to oscillations or maneuver of the aircraft induces a gyroscopical moment acting on the wing structure, thus changing its characteristic eigenbehavior. In case of the necessary guarantee for flight safety with regard to flutter, which is caused by the coupling of aero- and structural forces, the main concern is the change of the structural eigenbehavior due to gyroscopic moments [5]. Thus, the conventional flutter predictions are a subject to uncertainty since the influence is not clarified.

Previous work deals exclusively with the eigenbehavior of the system's stability with regard to flutter. Starting with a generic beam model, Runyan [6] pointed out the possible beneficial placing of masses to increase the flutter speed. Several research was done regarding the effect of an external store, to influence the system stability [7, 8], concluding the location of the mass being a sensitive parameter to the eigenbehavior. The exclusive influence of a follower force was demonstrated for a generic beam by Beck [9]. Hodges et al. [10] conducted the influence of a follower force however, suggested future work to realize the physical representation of an engine. One of the few contributions about gyroscopic influences was performed by Mazidi and Fazelzadeh [11] forcing a change of the angular momentum due to rolling maneuver. A flutter analysis was performed by Waitz and Hennings [5], showing the thrust and gyroscopic moments to influence the flutter speed critically. The principle influences are partially investigated from a system stability but not from a basis oriented structural-dynamical perspective. Furthermore, increasing simultaneously the engine geometry thereby, the mass and thus the angular momentum and the thrust, leads to yet unanswered questions about the structural load and structure coupling of the engine-wing system. The necessity of answering this concern is due to the need of thermodynamic optimization of the cycle process.

This paper presents two approaches from two different points of views. The thermodynamical modeling of both engines compares the cycle efficiency for specific design points. The structural dynamic part analyzes the consequence of the dramatic increase from a bypass ratio of 5 to 17. On the basis of a multibody formulation a model of a Coanda wing with the engine mounted on the airfoil and behind the wing (Fig. 1) of either bypass ratios and their influence on the wing are conducted.

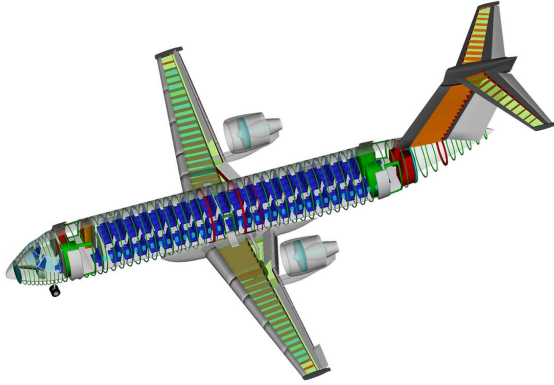


Figure 1. Reference configuration of the CRC 880 [12].

## 1. METHODS

### 1.1 Engine Cycle Design

In this study two different engine variants were designed. The first one is a conventional two spool turbofan with a BPR of 5 and OPR of 36, whereas the second configuration is an UHBR engine with a BPR of 17 and OPR of 70. The latter one is additionally equipped with a gearbox between the low pressure turbine (LPT) and the fan rotor. This allows the LPT to operate at higher and the fan rotor at lower speed level to run within its optimum range. Hence, the fan of a UHBR engine delivers a lower pressure ratio compared to one of a conventional engine.

Figure 2 shows the difference in cycles for a conventional and an UHBR engine. The lower FPR of the UHBR engine is also illustrated. Furthermore, Fig. 2 indicates the relationship between the turbine entry temperature (TET) and the OPR. In order to use efficiently the higher energy resulting from the higher TET, the compressors have to deliver a higher pressure ratio and therefore, the OPR in general has to be increased.

As a cycle design tool, the commercial software GasTurb 12 [13] was used. In GasTurb several engine cycles can be chosen, which is in the present work a conventional and a geared UHBR engine. By choosing the design point, ambient conditions, BPR, OPR, TET, component efficiencies serve as input parameters. Depending on the input parameters, the characteristic curves of each module, which are provided in GasTurb, are scaled to match the requirements. This can be supported by iteration procedures. In this study an iteration

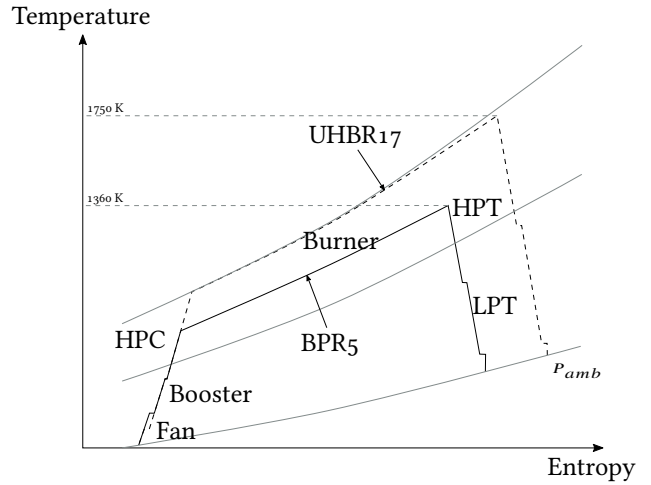


Figure 2. Cycle comparison between conventional turbofan and geared UHBR turbofan.

procedure was used to estimate mass flow and OPR for the required net thrust and OPR. The input component efficiencies were determined by extrapolating trends stated in Grieb [14] for a technology readiness level of 2015. This means that the materials are not necessarily used in 2015 but are available. A lower SFC for low pressure cycles, which is the case for an UHBR engine, is achieved when the nozzle velocities equal following component efficiencies [13]:

$$\left( \frac{V_{18,ideal}}{V_{8,ideal}} \right) = \eta_{fan} \cdot \eta_{LPT} \cdot \eta_{Gearbox}. \quad (1)$$

As already mentioned, top of climb operating point (case 1) was selected as the design point. In Tab. 1 all operating points are listed which the engines have to operate safely and efficiently. The off-design points include further common flight phases such as cruise (case 2), Take-off (case 5) and landing (case 8) where all engines are operating (AEO). However, safety relevant operating points in case of one engine inoperative (OEI) are also part of off-design cases (cases 3, 4, 6, 7, 9 and 10). Especially to be emphasized is the high power offtake during Take-off, approach and landing which is a result of the high-lift system required to Take-off and land at regional airports with a maximum runway length of 900 m.

For an adequate rotor dynamic analysis, realistic dimensions and hence, number of stages per module are crucial. Those are defined by the compressor pressure ratio (PR), for example 1.5 and 1.35 for an HPC respectively booster stage, [14]. Moreover, the HPC PR is the main driver for the OPR. In order to obtain inertia forces correctly a realistic mass estimation is necessary. The weight of the fan blades is supposed to have a large influence on the overall engine mass.

The density of the fan blades are estimated by assuming a share of 75% carbon fiber and 25 % titanium to withstand the impact of foreign object damage at blade leading edges.

**Table 1.** Flight and cycle parameters of both engines (BPR 5/UHBR 17).

Case	Operating Point	Height [m]	Mach [-]	Power Offtake [kW]	Bleed Air [kg/s]	Req'd Thrust [kN]
1	TOC, AEO	11277	0.74	11.8	0.44	18.8
2	Cruise, AEO,	11277	0.78	11.8	0.44	16.0
3	Take-off, OEI	11	0.17	764.9	0.88	71.7
4	Lift-off point, OEI	0	0.17	764.9	0.88	100.0
5	Take-off, AEO	0	0	382.5	0.44	129.9
6	Take-off, OEI	0	0	764.9	0.88	120.0
7	Approach, OEI	457	0.18	752.4	0.88	65.6
8	Landing, AEO	15	0.17	421.8	0.44	43.6
9	Landing, OEI	15	0.17	843.6	0.88	74.0
10	Cruise, OEI	5400	0.40	23.6	0.88	34.5
11	Cruise, AEO	12500	0.78	11.8	0.44	14.7

The most used titanium in aerospace application is Ti-6Al-4V, [15]. As a result of the increasing pressure and temperature, the materials in booster and HPC have to vary. Depending on the maximum temperature allowed various high temperature titanium alloys such as Timet 834 [16] are utilized in the front of the compressors whereas the latter stages of the HPC mainly use nickel-based alloys. Nickel-base alloys have a much higher density and hence, the weight increases faster than in case of titanium alloys. A high thermal stability is required in the combustion which only nickel-base superalloys are able to achieve, e.g. Hastelloy X [16]. The blade and vanes of the HPT operate under extreme conditions in an aero engine. In Bräunling [15] several examples are given for mono-crystalline superalloys. Reference [16] gives a few examples of cast and mono-crystalline nickel-base superalloys which can withstand temperatures higher than 1200 K. For LPT components  $\gamma$ -titanium aluminides are a choice as material due to its lower density and high ultimate tensile strengths up to about 1000 K [17].

## 1.2 Structural Dynamic Approach

The beneficial approach of a hybrid formulation is discussed in this chapter. Furthermore, the governing equations of a rotating system is presented.

### 1.2.1 Formalism of Modal Reduction

Assuming a linear and time invariant system with N degrees of freedom, the equations of motion to be reduced is stated as follows:

$$[M_{sy}]\{\ddot{u}\} + ([D_{sy}] + [D_{an}])\{\dot{u}\} + ([S_{sy}] + [S_{an}])\{u\} = \{p\} \quad (2)$$

With the aid of a time invariant transformation matrix T, which reduces the degrees of freedom N from the vector  $\{u\}$  to L of the vector  $\{v\}$ ,  $L \ll N$ :

$$\{v\} = [T]\{u\} \quad (3)$$

whereas  $[T] = \Phi$  consists of the eigenfrequencies and eigenvectors of the conservative system. The equations of motion (2) leads to

$$[T]^T [M] [T]^T \ddot{v} + [T]^T [D] [T]^T \dot{v} + [T]^T [S] [T]^T v = [T]^T \{p\} \quad (4)$$

respectively

$$[M]_{red}\{\ddot{v}\} + [D]_{red}\{\dot{v}\} + [S]_{red}\{v\} = \{p\}_{red} \quad (5)$$

### 1.2.2 Equations of Motion for the Rotating System

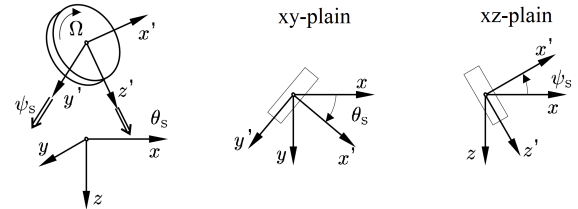


**Figure 3.** Coordinate system for a rotating mass.

For the present system, the main focus is on the antisymmetrical damping matrix  $[D_a]$  which only exists if gyroscopical moments are present. Considering a simple rotating disc (Fig. 3), the angular momentum in y-(6) and z-direction (7) is:

$$L_y = J_a \dot{\psi}_s - J_p \Omega \theta_s \quad (6)$$

$$L_z = J_a \dot{\theta}_s + J_p \Omega \psi_s \quad (7)$$

The resulting moment acting on the disc equals:

$$M_y = \frac{dL_y}{dt} = J_a \ddot{\psi}_s - J_p \Omega \dot{\theta}_s \quad (8)$$

$$M_z = \frac{dL_z}{dt} = J_a \ddot{\theta}_s + J_p \Omega \dot{\psi}_s \quad (9)$$

The respective first terms,  $J_a \ddot{\theta}_s$  (9) and  $J_a \ddot{\psi}_s$  (8), represent the inertia moments. Whereas each of the second terms,  $J_p \Omega \dot{\psi}_s$  (9) and  $-J_p \Omega \dot{\theta}_s$  (8), represent the gyroscopical moments due to a tilting and thus, a change in the angular momentum of the disc.

## 2. ENGINE PERFORMANCES

**Table 2.** Cycle parameters of the aero engine variant.

Parameter	Unit	BPR 5	UHBR 17
BPR	[-]	5	17
OPR	[-]	36	70
TET	[K]	1360	1750
FPR	[-]	1.81	1.41
GR	[-]	-	3.3
SFC	[g/Ns]	16.31	13.26

**Table 3.** Geometrical and physical parameters of both engines.

Components	Unit	BPR 5	UHBR 17
Fan	[-]	1	1
Booster	[-]	3	3
HPC	[-]	10	8
HPT	[-]	2	2
LPT	[-]	5	4
Gear	[-]	/	1
<b>Geom. Properties</b>			
Length <sub>Engine,max</sub>	[m]	3.76	3.27
Diameter <sub>Fan,max</sub>	[m]	1.75	2.26
Length <sub>Nacelle,max</sub>	[m]	2.83	2.17
<b>Phys. Properties</b>			
mass <sub>Engine,total</sub>	[kg]	1988.77	2088.06
mass <sub>Engine,rotating</sub>	[kg]	611.66	664.46
Inertia (LP/HP)			
$I_{1,rotating}$	[kgm <sup>2</sup> ]	54.52/3.9	141.9/1.9
$I_{2/3,rotating}$	[kgm <sup>2</sup> ]	435.6/16.5	235.3/4.7

### 2.1 Reference Engine

In recent engine designs for single-aisle aircrafts the BPR is around 5 which was selected as a reference. As stated above the OPR and TET have to be matched with the BPR. This led to an OPR of 36 and a TET of 1360 K, see Fig. 2. A FPR of 1.81 was estimated to achieve the required thrust at TOC operating point as stated in Tab. 1. However, all other off-design operating points are met as well. This results in a SFC of 16.31 g/Ns. The cycle parameters of the BPR 5 aero engine is summarized in Tab. 2.

The geometric design of the engine results in the number of stages per module listed in Tab. 3. The chosen architecture led to an engine weight of below 2000 kg.

### 2.2 Ultra-High Bypass Ratio Engine

The BPR of 17 for the UHBR engine is a result of a SFC and total engine weight sensitivity study. As described the higher BPR requires a much higher OPR, [4]. The trend for higher BPR (here 17) resulting in larger OPR (70) and lower FPR (1.41) is confirmed as depicted in Fig. 2. Again, this is in compliance with engine designs from Daggett et al. [3], which also had a technology readiness level of 2015. The SFC of 13.26 g/Ns is also in accordance to ref. [4].

The total engine mass with above 2000 kg is slightly higher compared to the BPR 5 engine which is mainly a result of the additional gearbox. Nevertheless, this is compensated by the lower fuel consumption with regard to the aircraft operating costs.

### 2.3 Multibody Model

The multibody was topologically built up in two versions, one model with the conventional engine with a bypass ratio of 5, the other one with the ultra high bypass ratio of 17 (Fig. 5). Both versions used the Coanda wing from [18] (Fig. 4). The properties of the wing are presented in [19]. The model of the pylon features no dynamical behavior, thus the wing and the engines are connected with a rigid body. This assumption is a first in the series of iterations to the more accurate resolution. A comparison of the significant properties and components describing both engines are presented in Tab. 3. Both engines consist of a fan (LP), booster, HPC, HPT, LPT. The main difference in the constructional concept is the planetary gear (GR = 3.30) in the UHBR gas turbine to step down the rotational velocity of the LP shaft.

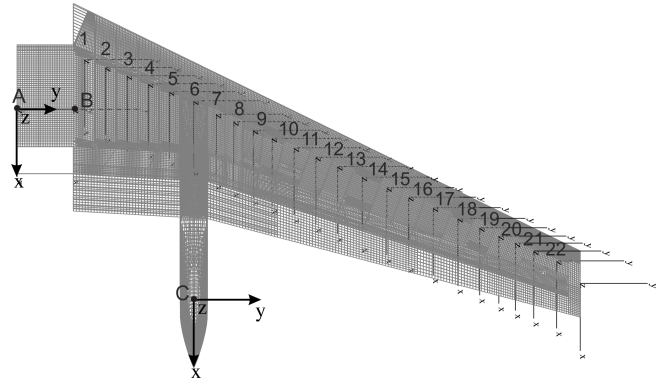


**Figure 4.** MBS model of the Coanda wing.

## 3. RESULTS AND DISCUSSION

In the following section the results of the multibody simulations are presented. At first, the time dependent behavior of the multibody model is evaluated by simulating a realistic startup.

At second, the behavior of the wing-engine system is investigated in the frequency domain by inducing different types of excitations on the system. Two different operating points were simulated.

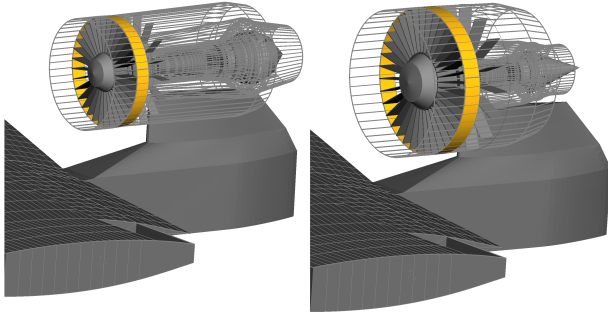


Figure 5. MBS model, left: BPR 5, right: UHBR 17.

On the one hand, the *TOC* with regard to the *SFC* and on the other hand the *Take-off* with regard to the *ROM* [20] were chosen in particular.

### 3.1 Time Dependent Behavior

#### 3.1.1 Startup Simulation

A critical procedure for gas turbines is the startup. With regard to resonance, during the increase of the rotational velocity, eigenfrequencies of the system, especially of the gas turbine itself, can be excited, thus leading to large amplitudes of the structure due to the resonance. To ensure safety, a realistic startup was simulated by increasing the rotational velocity of the LP shaft from 0 RPM to 55% of  $\Omega_{max,LP}$  (respectively the fan and HP shafts with according rotational velocity) within 30 seconds followed by a 5 second interval of constant rotational velocity (Fig. 6).

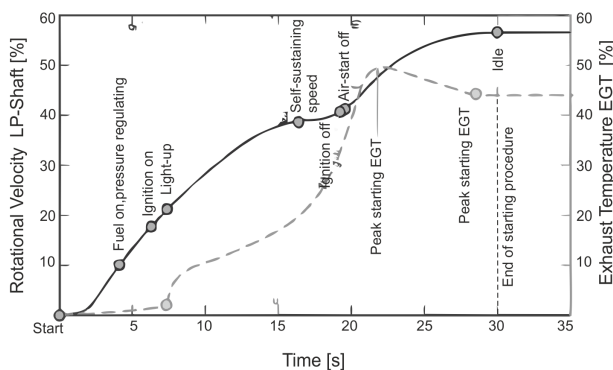


Figure 6. Startup procedure [15].

Two approaches to analyze the influence of the different engine models were chosen. On the one hand the wing root was evaluated by analyzing the absorbed force/torque by the fuselage (represented by the constraints at the joint).

On the other hand the movement of the wing itself (in *z*-direction) to evaluate the deflection.

The results of the torque in each spatial direction are depicted in Fig. 7. Both models show a similar behavior in their results.

With advancing time the magnitude of the torque increases due to the higher rotational velocity. The increase, however, in *z*-direction increases overly proportional compared to the other two directions towards the end of the startup.

Qualitative spoken, for each model, the oscillation of the torque in *x*- and *y*-direction have the same behavior over the time in phase. Thus the high frequencial behavior does not influence the global wing behavior/load. The structure in *z*-direction is autonomously excited and shows no explicit in- or dephasing behavior compared to the other directions. This is due to the fact that in *z*-direction is an additional constraint at point **B** (Fig. 4), whereas in the *x*- and *y*-direction all degrees of freedom are provided. In case of the BPR 5 after  $\sim 0.6$  s the increase of the amplitude is due to the excitation of the eigenfrequency of the wing. The second excitation occurs around  $\sim 15$  s when the LP shaft is excited. The later increase of the amplitude is solely due to the increase of the rotational velocity/angular momentum. In case of the UHBR 17 the same excitation at the beginning occurs. In contrast to the BPR 5 the fan shaft is excited. Starting at  $\sim 5$  s the first eigenfrequency is excited and thus the amplitude increases. It decays after  $\sim 18$  s, however, due to the increase of the rotational velocity after  $\sim 20$  s the amplitude increases again till the end of the startup.

In the interval from 30 s to 35 s, in which the rotational velocity is held constant, the maximum amplitude, in *x*- and *y*-direction, of the PBR 5 case is  $\sim 2.3$  times higher than the one of the UHBR 17 case. The primary reason is the fact that the rotational velocity of the low-pressure unit is near an eigenfrequency of the system. An additional reason is, despite the fact that the UHBR 17 engine possesses a 1.78 higher angular momentum, the higher amplitude results due to the 13.7%, in relation to the UHBR 17 engine, farther center of gravity from the wing axis and thus possesses a longer lever arm.

Normalizing the torque [Nm] to the actual resulting angular momentum [ $\text{kgm}^2/\text{s}$ ] of the rotating gas turbine shafts serves as a ratio of structural consequence based on the energetic input,  $\frac{\text{Output}_{\text{Structure}}}{\text{Input}_{\text{Energy}}}$ . The ratio of the angular momentum of both engines  $\frac{L_{\text{UHBR17}}}{L_{\text{BPR5}}}$  equals 1.78. Qualitatively spoken, the behavior of both engines do not change, due to the fact that the factor is only dependent on  $\Omega$ . The results of the normalized torque (Fig. 8) show high amplitudes at the beginning, which is feasible because the angular momentum is very small at the beginning. However with increasing angular momentum, comparing the results in *z*-direction, the amplitudes of both models increase.

Whereas the one from the BPR 5 engine increases over proportionally compared to the UHBR 17 engine. In other words the higher bypass ratio, thus, the higher angular momentum, does not lead to an equal proportional load increase.

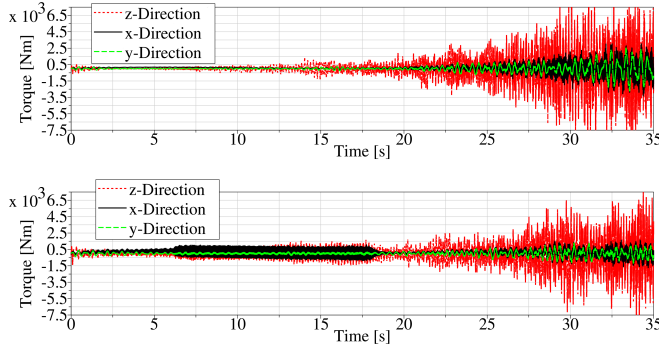


**Figure 7.** Torque at the wing root (Point A Fig. 4) for the respective directions. Top: BPR 5, Bottom: UHBR 17.

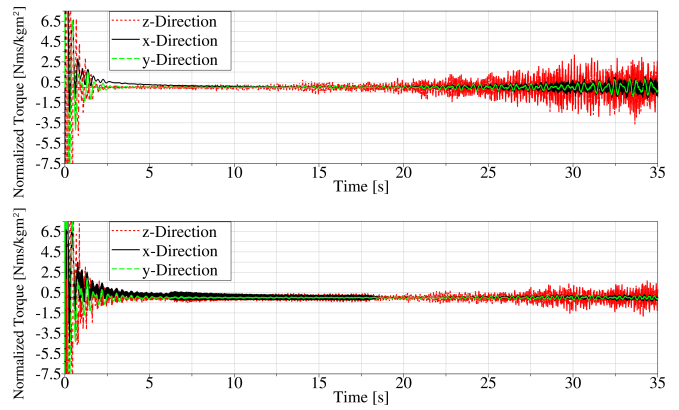


**Figure 8.** Normalized torque at the wing root (Point A Fig. 4) for the respective directions. Top: BPR 5, Bottom: UHBR 17.

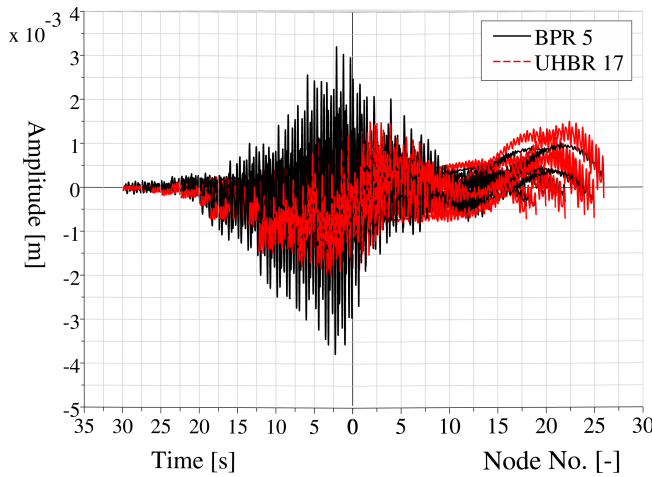


**Figure 9.** Sliding mean value of the amplitude over the time for nodes no.1-22 (in spanwise direction) on the Coanda wing Fig. 4.

The structural dynamic consequences for the wing was evaluated by analyzing the time dependent behavior of the wing at specific points (Fig. 9). The results for the amplitude (mean value over 1s in z-direction) over the simulation duration at each node is presented in Fig. 9.

Reasonably, the amplitudes of both models grow towards the wing tip (in spanwise/y-direction). Due to the excitation of the fan shaft at the beginning of the startup procedure the maximum amplitude for the UHBR engine is twice as big as the one from the conventional one. The same ratio applies to the values for the amplitude towards the end of the simulation, however in this case the higher amplitudes are not caused by an excitation but by the increased angular momentum.

### 3.2 Frequency Dependent Behavior

The system response in the frequency domain due to different external excitations was evaluated for two cases: the design point - *TOC* and an off-design point - *Take-off* and

the response, in form of the force in z-direction at the wing root (at point **B** Fig. 4). Therefore the wing tip was excited with a frequency from 1 Hz to 250 Hz with an amplitude of 1 N. With regard to the system response the amplitude has only a subordinate role due to the fact that the equations, in this case, are solved linear. The focus is on the relative ratio of the individual excited frequencies. Additionally an unbalance force (10):

$$F_{unbalance} = m_u d \cdot \Omega^2 \quad (10)$$

at the fan and the rear bearings of the HP and LP shafts excited the gas turbine separately, with  $m_u d = 10^{-4}$  kgm. The operating parameters are listed in Tab. 4.

**Table 4.** Operating parameters.

TOC	Unit	UHBR 17	BPR 5
HP	[rpm]	18020	13823
LP	[rpm]	9235	5769
Fan	[rpm]	2806	5769
Thrust	[kN]	18.8	18.8
Take-off			
HP	[rpm]	20147	16381
LP	[rpm]	9422	6855
Fan	[rpm]	2863	6855
Thrust	[kN]	129.9	129.9

The following applies to all evaluations. As force /vibration transmission to the fuselage all results were evaluated at point **B** Fig. 4.

The results are depicted as the relationship of  $\frac{\text{Output}}{\text{Input}}$  which corresponds to the system response characteristics. Amplitudes below  $10^0$  were not considered, therefore, the spectrum ranges from 0 Hz to 60 Hz.

### 3.2.1 Wing Tip Excitation

The predominant movement of a wing is a flap-motion and the most common flutter coupling a bending-torsion of the wing, thus the chosen excitation simulated a forced flap with the excitation point at the wing tip. The results are shown in Fig. 10.

For a comparison with the original eigenvalues from the clean wing and the change due to the modeling of the engine, the spectrum of the *clean wing* is depicted as well. As expected, the excited amplitudes decrease with higher frequency while only the bending modes are excited. Adding an additional mass to the wing causes in terms of an engine the original frequencies corresponding to bending mode shapes to split up, resulting in not only pure bending but bending with torsion and in-plane movement. The corresponding frequencies for the excited peaks are listed in Tab. 5 and a comparison of the change in the frequency/amplitude compared for both cases.

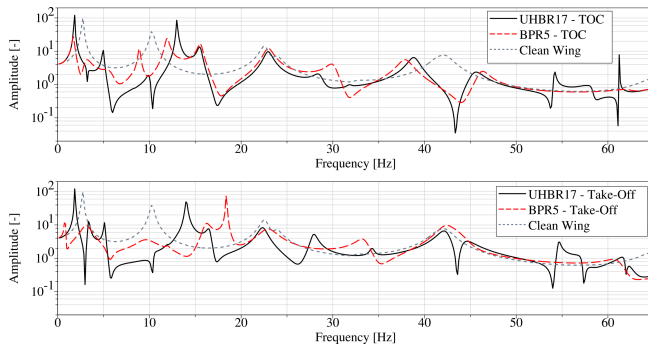


**Figure 10.** Comparison of the root force with excited wing tip. Top: *TOC*, Bottom: *Take-off*.

Each excited peak can be qualitatively, by evaluating the mode shape, traced back to the original mode shape of the clean wing. For example peak 1 and 2 correspond to the first original peak (for both engines) or the two peaks around 42 Hz originating from it. For the case *TOC* the UHBR 17 engine shows significantly higher amplitudes of the excited peaks, number 1 and 5, compared to the corresponding peaks of the BPR 5 engine. With increasing frequency the amplitudes of both engines spectra decrease in a similar way. Regarding the *Take-off* point the high sensitivity to the rotational velocity of both models, especially the one of the BPR 5 engine, needs to be pointed out. The increased thrust has only a marginally effect on the change of the eigenvalues, whereas the increased rotational velocity and thus, the higher angular momentum primarily shifts the eigenfrequencies significantly. In case of the UHBR 17 engine the LP/HP/fan shafts only rotate 2%/11.8%/2% faster.

Whereas in case of the BPR 5 engine the LP/HP/fan shafts rotate 18%/18%/18% faster. Still the relative system response is in favor of the BPR 5 engine showing smaller responses to the disturbances.

**Table 5.** Excited eigenfrequencies (*TOC* / *Take-off*).

Peak No.	BPR 5		UHBR 17	
	Freq. [Hz]	Ampl. [-]	Freq. [Hz]	Ampl. [-]
1	1.7/0.7	27.3/11.6	1.9/1.9	123.0/124.3
2	3.2/3.1	5.6/9.6	-/3.3	-/13.1
3	8.9/9.6	11.9/3.6	4.9/5.1	10.8/11.9
4	11.9/16.2	23.3/11.2	9.9/-	1.9/-
5	15.5/18.3	16.8/75.3	12.9/13.9	87.3/50.3
6	22.9/22.9	11.8/7.6	15.5/16.5	13.6/7.7
7	29.9/33.2	4.1/3.8	22.8/22.2	9.5/8.1
8	37.9/42.5	5.6/9.7	28.3/27.9	2.1/5.3
9	46.3/-	2.5/-	38.7/42.1	6.4/6.6

### 3.2.2 Unbalance Excitation - *TOC* - Case 1

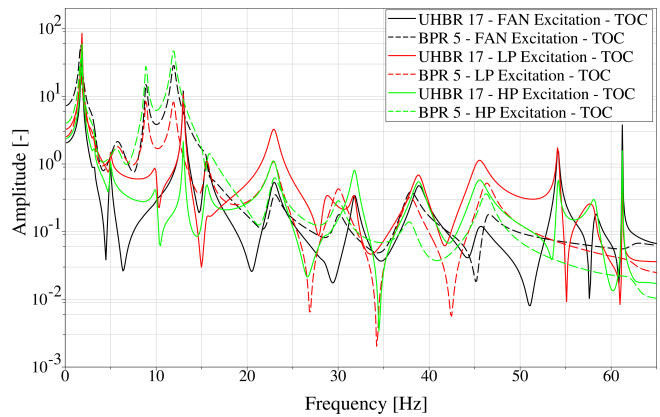


**Figure 11.** Comparison of the root force in z-direction for the design point *TOC*.

The results for the unbalance force for the case *TOC* are presented in Fig. 11. For either, the UHBR 17 and the BPR 5 engine as well, all eigenfrequencies of the wing with a participation of a bending mode are excited due to the unbalance forces.

In case of the UHBR 17 engine the primarily excited peak, at 1.85 Hz, has the highest amplitude with the unbalance situated at the LP shaft. In principle, this statement generally applies to all cases. Even though the HP shaft rotates with  $\sim 2.2$  time the velocity of the LP shaft, the resulting angular momentum of the LP shaft compensates this 11.6 times higher rotary inertia. Only for the last frequency in the spectrum at 61.2 Hz, which corresponds to the first eigenfrequency of the fan, is this statement not valid. In case of the fan excitation this amplitude plausibly stands out.

In case of the BPR 5 engine the first peak, at 1.72 Hz, the third, at 8.85 Hz, and the fourth peak, at 11.85 Hz, dominates the spectrum and not only a single one in case of the UHBR 17 engine. The most serious influence on the system response behavior is caused by the HP excitation.

Due to the fact, that no planetary gear reduces the rotational velocity the influence of the fan, however, is obviously greater than the one of the LP shaft. This applies for the LP excitation in case of the UHBR 17 and for the HP excitation in case of the BPR 5 engine.

By comparing the values of the spectra of the UHBR 17 and the BPR 5 engine with each other, the considerable larger amplitudes of the BPR 5 and thus, the advantage of the UHBR 17 engine can be seen in Tab. 6:

**Table 6.** RMS amplitudes of both engine approaches for *TOC*.

	UHBR 17	BPR 5	$\frac{UHBR17}{BPR5}$
<b>LP</b>	791.04	502.11	1.57
<b>HP</b>	380.95	1043.44	0.36
<b>Fan</b>	310.99	967.55	0.32

### 3.2.3 Unbalance Excitation - Take-off - Case 5

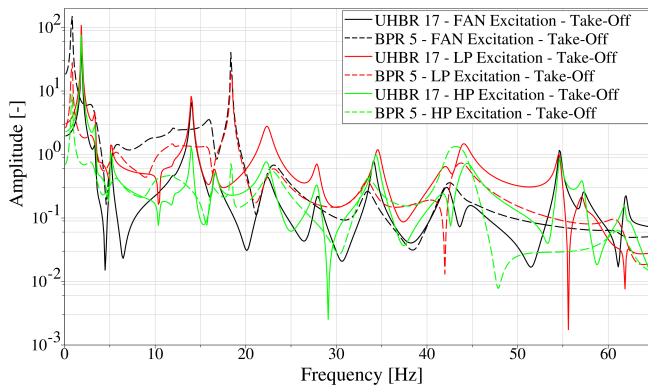


**Figure 12.** Comparison of the root force in z-direction for the off-design point *Take-off*.

The results for the unbalance force for the case *Take-off* are presented in Fig. 12. The sensitivity of rotational velocity and thus, shifting of sensitive eigenfrequencies can be observed, [19]. For the UHBR 17 engine, only the HP shaft increases for 11.8%, whereas the LP and fan only increase their rotational velocity by 2%.

Noteworthy is the strong decrease of the last peak, which arises due to the excitation by the fan and vanishes nearly. The characteristics of the BPR 5 engine change dramatically. The first eigenfrequency shifts from 1.72 Hz to 0.85 Hz and increases strongly in amplitude. The third and fourth peak vanishes, whereas a peak at 18.35 Hz arises, which is a coupling of the wing with the LP/fan shaft.

The influence of the HP shaft nearly vanishes through the response spectrum and is dominated by the fan/LP shaft characteristics. This can be seen in the comparison of the RMS values of the amplitudes presented in Tab. 7. As in the case before, looking at the worst case scenario, the maximum amplitude overall is caused by the BPR 5 engine.

**Table 7.** RMS amplitudes of both engine approaches for *Take-off*.

	UHBR 17	BPR 5	$\frac{UHBR17}{BPR5}$
<b>LP</b>	814.68	473.15	1.72
<b>HP</b>	389.25	189.71	2.05
<b>Fan</b>	305.09	1049.84	0.29

## 4. CONCLUSION

In the paper two different aero engines are developed: The first one is a conventional engine with a BPR of 5 and serves as a reference for both the thermodynamic cycle design as well as for the structural dynamic comparison.

The second variant is a future-oriented aero engine with a BPR of 17 with a so-called ultra-high bypass ratio. The first part of the paper describes the design of the engines. Thereby, special attention has been drawn on the component design, that PR and efficiencies represent a technology level reached in the year 2015. It has to be emphasized that the BPR has to be carefully matched with the OPR, TET and FPR to attain lower SFC for the UHBR engine. A reduction of 18.7 % in SFC was achieved for an UHBR engine compared to a conventional engine. Furthermore, component materials (also with a technology level reached in 2015) were selected to represent realistic geometry and mass estimation which is from great importance for the multibody modeling. For all engine modules the preferable and most frequently used materials in aero engine construction are presented based on literature references. The materials differ in strength and operating temperatures. Structural dynamic consequences on the wing due to the rotating components were investigated using hybrid multibody models. The time dependent simulations could not support the assumption of a fundamental negative trade-off by the increased diameter of the fan. Within the simulation of a startup procedure the transmitted load to the fuselage is relatively less by the UHBR 17 engine compared to the BPR 5 engine. The evaluation in the frequency domain by investigating the system response behavior to disturbances was simulated by an unbalance force situated at different locations within the gas turbine. The comparison of the results of two different operating points, the *TOC* and the *Take-off*, were in favor of the UHBR 17 engine. Looking at the worst case scenario the highest system responses were generated by the BPR 5 engine.

In case of the *TOC* 31.9% and for the *Take-off* 28.9% higher amplitudes of the BPR 5 compared to the UHBR 17 engine. A substantial influential factor in the dynamical behavior, due to the required design, is presumable the pylon construction its attributed degrees of freedom and physical properties. Hence future work will include a flexible model of the pylon. Additionally, regarding the system stability, aerodynamical forces will be included to conduct a flutter analysis. In this sense an aerodynamic model in the form of a strip theory is developed and implemented in simpack.

## ACKNOWLEDGMENTS

The authors gratefully acknowledge the funding as part of the Coordinated Research Centre 880 (Sonderforschungsbereich 880, SFB 880) provided by the German Research Foundation (Deutsche Forschungsgemeinschaft).

## REFERENCES

- [1] Advisory Council for Aeronautics Research In Europe (ACARE). A vision for 2020. 2001.
- [2] Advisory Council for Aeronautics Research In Europe (ACARE). Flightpath 2050 - europe's vision for aviation. 2011.
- [3] D. L. Dagget and S. T. Brown. Ultra-efficient engine diameter study. *NASA/CR-2003-212309*, 2003.
- [4] C. A. Hall and D. Crichton. Engine design studies for a silent aircraft. *Journal of Turbomachinery*, 129(3):479–487, 2006.
- [5] S. Waitz and H. Hennings. The aeroelastic impact of engine thrust and gyroscopics on aircraft flutter instabilities. *IFASD*, 2015.
- [6] H. L. Runyan and C. E. Watkins. Flutter of an uniform wing with an arbitrarily placed mass according to a differential-equation analysis and a comparison with experiment. *NACA Technical Report*, 1950.
- [7] H. L. Runyan. Effect of a flexible mounted store on the flutter speed of a wing. *NASA Contractor Report*, 1980.
- [8] F. H. Gern and L. Librescu. Effect of externally mounted stores on aeroelasticity of advanced swept cantilevered aircraft wings. *Aerospace Science and Technology*, (5):321–333, 1998.
- [9] M. Beck. Die Knicklast des Einseitig eingespannten, tangential gedrückten Stabes. *Journal of Applied Mathematics*, 3:225–228, 1952.
- [10] D. H. Hodges, M. J. Patil, and S. Chae. Effect of thrust on bending-torsion flutter of wings. *Journal of Aircraft*, 39(2), 2001.
- [11] A. Mazidi and S.A. Fazelzadeh. Flutter of aircraft wings carrying a powered engine under roll maneuver. *Journal of Aircraft*, 2011.
- [12] R. Radespiel and W. Heinze. Sfb 880: Fundamentals of high lift for future commercial aircraft. *Council of European Aerospace Societies Journal*, 5(239-251), 2013.
- [13] J. Kurzke. *GasTurb 12 - Design and Off-Design Performance of Gas Turbines*.
- [14] H. Grieb. *Verdichter fuer Turbo-Flugtriebwerke*. Springer-Verlag, 2009.
- [15] W. J. G. Bräunling. *Flugzeugtriebwerke*. Springer, 2009.
- [16] N. R. Muktinatalapati. *Advances in Gas Turbine Technology*, chapter Materials for Gas Turbines - An Overview, pages 593–314. InTech, 2011.
- [17] V. Recina and B. Karlsson. High temperature low cycle fatigue properties of ti-48al-2w-0.5si gamma titanium aluminide. *Materials Science and Engineering*, 262:70–81, 1999.
- [18] K. Sommerwerk, B. Michels, K. Lindhorst, M.C. Haupt, and P. Horst. Application of efficient surrogate modeling to aeroelastic analyses of an aircraft wing. *Aerospace Science and Technology*, 55:314–323, 2016.
- [19] T. S. Mueller and H. Hennings. Structural dynamic influence of an UHBR engine on a coanda-wing. *IFASD*, 2017.
- [20] I. Krukow and D. Dinkler. A reduced-order model for the investigation of the aeroelastic of circulation-controlled wings. *Council of European Aerospace Societies Journal*, 5(2):145–156, 2014.